Acta Crystallographica Section B
Structural Science
ISSN 0108-7681

Reversible phase transition of pyridinium-3-carboxylic acid perchlorate

Heng-Yun Ye,* Li-Zhuang Chen and Ren-Gen Xiong

Ordered Matter Science Research Center, Southeast University, Nanjing 211189, People's Republic of China

Correspondence e-mail: hyye@seu.edu.cn

Received 11 October 2009
Accepted 27 April 2010

Pyridinium-3-carboxylic acid perchlorate was synthesized and separated as crystals. Differential scanning calorimetry (DSC) measurements show that this compound undergoes a reversible phase transition at ~ 135 K with a wide hysteresis of 15 K. Dielectric measurements confirm the transition at ~ 127 K. Measurement of the unit-cell parameters *versus* temperature shows that the values of the c axis and β angle change abruptly and remarkably at 129 (2) K, indicating that the system undergoes a first-order transition at $T_c = 129$ K. The crystal structures determined at 103 and 298 K are all monoclinic in $P2_1/c$, showing that the phase transition is isosymmetric. The crystal contains one-dimensional hydrogen-bonded chains of the pyridinium-3-carboxylic acid cations, which are further linked to perchlorate anions by hydrogen bonds to form well separated infinite planar layers. The most distinct differences between the structures of the higher-temperature phase and the lower-temperature phase are the change of the distance between the adjacent pyridinium ring planes within the hydrogen-bonded chains and the relative displacement between the hydrogen-bonded layers. Structural analysis shows that the driving force of the transition is the reorientation of the pyridinium-3-carboxylic acid cations. The degree of order of the perchlorate anions may be a secondary order parameter.

1. Introduction

The role of hydrogen bonds in temperature-driven structural phase transitions is of current interest (Horiuchi *et al.*, 2007). For example, Szafranski *et al.* (2002) have reported some genuine ferroelectric analogues of KH_2PO_4 (KDP): the 1,4-diazabicyclo[2.2.2]octane (dabco) salts with inorganic anions. The mono-protonated amines ($Hdabco^+$ cations) form an infinite chain containing disordered short homonuclear N—$H^+\cdots$N bonds in the paraelectric phase. The paraelectric-to-ferroelectric phase transition is triggered by the collective ordering of protons upon lowering the temperature (Katrusiak & Szafranski, 1999). The mono-protonated pyrazine compounds also show a similar phase transition mechanism to the dabco monosalts (Katrusiak & Szafranski, 2006). More recently, Horiuchi *et al.* (2005) have developed new ferroelectric organic solids, the cocrystals of phenazine (Phz) with chloranilic acid (H2ca) and bromanilic acid (H2ba), in which nonpolar neutral molecules are connected by the intermolecular O—H$\cdots$N hydrogen bonds. The driving forces of the phase transition were shown by neutron diffraction to be the displacements of H atoms (Kumai *et al.*, 2007). Compared with these strong hydrogen-bonding interactions, weak

Table 1
Crystal data for (I) at 103, 148 and 298 K.

For all structures: M_r = 223.57, Z = 4. Experiments were carried out with Mo $K\alpha$ radiation using a Saturn724+ (4 × 4 bin mode) diffractometer.

	103 K	148 K	298 K
Crystal data			
Chemical formula	$C_6H_6{\cdot}ClNO_6$	$C_6H_6{\cdot}ClNO_6$	$C_6H_6{\cdot}ClNO_6$
Crystal system, space group	Monoclinic, $P2_1/c$	Monoclinic, $P2_1/c$	Monoclinic, $P2_1/c$
a, b, c (Å)	7.4564 (10), 16.5261 (18), 7.1282 (8)	7.404 (6), 16.793 (11), 7.751 (6)	7.400 (7), 16.996 (13), 7.865 (7)
β (°)	79.754 (4)	112.817 (10)	112.717 (12)
V (Å^3)	864.37 (18)	888.3 (11)	912.4 (13)
μ (mm^{-1})	0.45	0.44	0.42
Crystal size (mm)	0.45 × 0.40 × 0.40	0.45 × 0.40 × 0.40	0.45 × 0.40 × 0.40
Data collection			
Absorption correction	Multi-scan *CrystalClear* (Rigaku, 2005)	Multi-scan *CrystalClear* (Rigaku, 2005)	Multi-scan *CrystalClear* (Rigaku, 2005)
T_{min}, T_{max} (normalized)	0.877, 1.000	0.877, 1.000	0.867, 1.000
No. of measured, independent and observed [$I > 2(I)$] reflections	8182, 1971, 1772	9255, 2013, 1823	9560, 2075, 1803
R_{int}	0.039	0.028	0.033
Refinement			
$R[F^2 > 2(F^2)]$, $wR(F^2)$, S	0.036, 0.098, 1.07	0.059, 0.147, 1.09	0.077, 0.216, 1.06
No. of reflections	1971	2013	2075
No. of parameters	128	141	141
No. of restraints	0	6	0
H-atom treatment	H-atom parameters constrained	H-atom parameters constrained	H-atom parameters constrained
$\Delta\rho_{max}$, $\Delta\rho_{min}$ (e Å^{-3})	0.44, −0.55	0.82, −0.57	0.64, −0.48

Computer programs used: *CrystalClear* (Rigaku, 2005), *SHELXTL* (Sheldrick, 2008), *DIAMOND* (Brandenburg & Putz, 2005).

hydrogen-bonding interactions (Steiner, 1996) have received much less attention, although their changes may contribute to the phase transitions (Chantrapromma *et al.*, 2006; Usman *et al.*, 2001).

Nicotinic acid, as an amino acid, is a good material to construct hydrogen-bonded structures consisting of protonated amino acids with different inorganic anions like triglycine sulfate (TGS). Some nicotinium salts with inorganic anions, such as nicotinium nitrate monohydrate (Jebas *et al.*, 2006), dinicotinium sulfate (Athimoolam & Rajaram, 2005*b*), nicotinium dihydrogenphosphate (Athimoolam *et al.*, 2005), 3-carboxypyridinium chloride (Slouf, 2001) and bis(nicotinic acid) hydrogen perchlorate (Athimoolam & Rajaram, 2005*a*), have been reported previously. Their crystal structures involve a variety of hydrogen-bond modes. However, no further investigations on their phase-transition properties have been reported. As a continuation of our study (Chen *et al.*, 2009) on phase transitions involving hydrogen-bond systems, we studied the phase transition properties of pyridinium-3-carboxylic acid perchlorate (I) by single-crystal X-ray analysis, differential scanning calorimetry (DSC) and dielectric measurements.

2. Experimental

2.1. Synthesis

Pyridinium-3-carboxylic acid perchlorate (I) was obtained as crystals by evaporation of an aqueous solution containing equal molar quantities of perchloric acid and 3-pyridinecarboxylic acid at room temperature. The IR spectrum (see supplementary material,[1] Fig. 1S) of (I) definitely displays the existence of the typically strong vibration peaks of ClO_4^- between 1150 and 1100 cm^{-1}. The powder XRD (PXRD) pattern of (I) at room temperature matches very well the pattern simulated from the single-crystal structure (see supplementary material, Fig. 2S).

2.2. Crystallography

Crystallographic data were collected using a Rigaku Saturn 724+ diffractometer equipped with a Rigaku low-temperature gas-spray cooler, with Mo $K\alpha$ (λ = 0.71075 Å) radiation from a graphite monochromator. The crystal temperature was stable to within 2−5 K. Data processing including empirical absorption correction was performed using the *CrystalClear* software package (Rigaku, 2005). The structures were solved by direct methods and successive Fourier synthesis and then refined by full-matrix least-squares refinements on F^2 using the *SHELXLTL* software package (Sheldrick, 2008). Non-H atoms were refined anisotropically using all reflections with $I > 2\sigma(I)$. For structures at 148 and 298 K, the perchlorate anion is disordered in two orientations with site-occupancy factors of 0.832 (4) and 0.178 (4), 0.809 (3) and 0.191 (3), respectively; the anisotropic displacement parameters for the two parts of each O atom were constrained to be equal. All H atoms were found in the difference maps. However, they were placed at ideal positions and refined using a 'rotating' model for the hydroxyl H atom with U_{iso} = 1.5 U_{eq} (O) and a 'riding' model

[1] Supplementary data for this paper are available from the IUCr electronic archives (Reference: HW5007). Services for accessing these data are described at the back of the journal.

for the other H atoms with U_{iso} = 1.2 U_{eq} (C or N). The asymmetric units were drawn with *SHELXLTL* and the packing views were drawn with *DIAMOND* (Brandenburg & Putz, 2005) *Visual Crystal Structure Information System* software. The distances between planes were calculated using *DIAMOND* and the other calculations were carried out using *SHELXLTL*. Crystallographic data and details of the data collection and refinement for the structures at 103, 148 and 298 K are given in Table 1.

2.3. DSC measurements

DSC measurements were performed by heating and cooling the samples (25.2 mg) in the temperature range 93–373 K on a Perkin–Elmer Diamond DSC instrument. The measurements were carried out under nitrogen at atmospheric pressure in aluminium crucibles with a heating rate of 5 K min^{-1}.

2.4. Dielectric measurements

The complex permittivity ε ($\varepsilon = \varepsilon' - i\varepsilon''$) was measured with a Tonghui TH2828A impedance analyzer in the frequency range 10–1000 kHz. The measuring AC voltage was 1 V. The pressed-powder pellet (0.44 mm thick and 17.3 mm^2 in area) deposited with silver-conducting glue was used for dielectric studies.

3. Result and discussion

3.1. Differential scanning calorimetry

The phase transition was first detected by DSC measurements. Upon heating and cooling, the crystalline sample undergoes a single phase transition at *ca* T_c = 135 K, showing an endothermic peak at 135.6 K and an exothermic peak at 120.7 K (Fig. 1). These observed peaks represent a reversible phase transition with a 15 K hysteresis. The sharp peaks and thermal hysteresis reveal the discontinuous character of the transition, being indicative of a first-order phase transition.

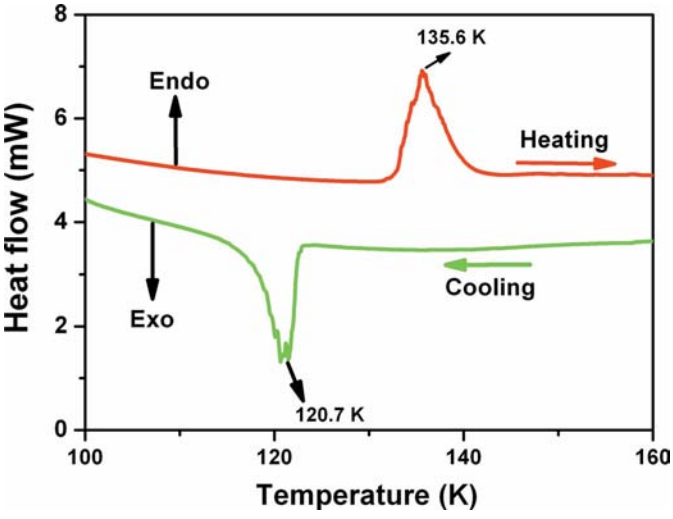

Figure 1
DSC curves for (I).

3.2. Dielectric properties

The variable-temperature dielectric response, especially in a relatively high frequency range, is very useful for searching for phase transitions. Owing to the difficulty of growing large crystals, a pressed-powder pellet of (I) was used in dielectric measurements. The temperature dependences of the real part of the dielectric permittivity and the dielectric loss taken at 10, 100 and 1000 kHz are shown in Fig. 2. The occurrence of a dielectric anomaly in the real part of the dielectric permittivity at each frequency shows the phase transition at *ca* 127–135 K to be consistent with the DSC result, within experiment error. Both the real and imaginary parts of the dielectric permittivity show a frequency dependence due to dielectric relaxation. Usually, in the low-frequency range the temperature of the dielectric anomaly should match well with that observed in cooling-mode DSC, which means T_c is close to 127 K. We also performed the dielectric measurements on pressed powder pellets of the other nicotinium salts containing different inorganic anions such as BF_4^-, PF_6^-, NO_3^-, SO_4^{2-}, Cl^-, Br^- *etc.*, but no distinct dielectric anomaly was observed.

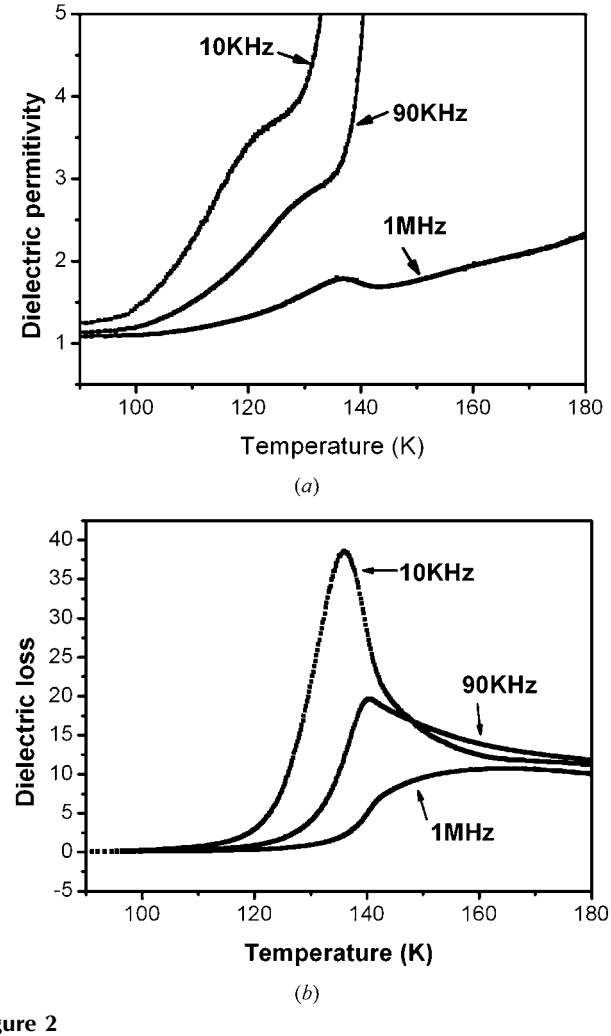

Figure 2
Temperature dependences of the real part of the permittivity (*a*) and the dielectric loss (*b*) of (I) at 10–1000 kHz.

3.3. Structure and crystal packing

In order to understand the phase transition, the structures of (I) were determined at 103, 148 and 298 K. The structure determined at 148 K, a little above T_c, shows that the higher-temperature phase (HTP) is monoclinic $P2_1/c$ with the cell parameters $a = 7.40$, $b = 16.79$, $c = 7.75$ Å and $\beta = 112.81°$, very similar to those at 298 K. The lower-temperature phase (LTP) structure determined at 103 K is also monoclinic $P2_1/c$ with a and b axis lengths similar to those in the HTP, but it shows a modest change in the length of the c axis ($c = 7.12$ Å) and a large change in β angle ($\beta = 100.25°$). Therefore, the phase transition is isosymmetric, but c and the β angle change significantly.

For the lower-temperature (LT) structure, a common origin and axial directions similar to those of the higher-temperature (HT) structure should be chosen, to keep the same molecular orientation and hence facilitate the comparison of the structural changes. It is known that in most cases cell parameters and the displacements of atoms change little during a structural phase transition that leaves the crystal intact. In this case, however, the large changes of the cell parameters make it difficult to determine the most likely relationship between the HTP and LTP. Two possibilities for the cell of the LTP have been considered.

The first possibility is the standard reduced cell of the LTP. Figs. 3 and 4 show the diagrams of cell packing at 148 (the minor part of the disordered perchlorate anions was omitted for clarity) and 103 K viewed down the c and b axis, respectively, where the corresponding pyridinium-3-carboxylic acid cations have similar orientations but the orientations of the corresponding perchlorate anions look different. When further comparing the hydrogen-bonded layers (Fig. 5), the cations in the two phases tilt in different directions and the orientations of the anions are different. A second possibility is that the **b** and **c** directions in the LT structure are opposite those of the HT structure. This leads to a second unit-cell setting for the LT structure, with a β angle of 79.75° which is the supplement of the β angle of the reduced cell. As shown in Figs. 6 and 7, both the cations and anions have similar orientations when the second unit-cell setting is chosen for the LT structure. However, when viewed down the b axis (Fig. 8) it is clear that the relative displacement between the layers along the a axis is rather large, owing to the large change of the β angle from 112.81 to 79.75° during the phase transition. Although rather large displacement between the layers is required if the two structures are related in this way, all the shifts within a hydrogen-bonded layer are similar which will be discussed below in more detail. Usually a pair of phases in which layers are stacked somewhat differently is easier to understand than a pair of phases in which reorientations of

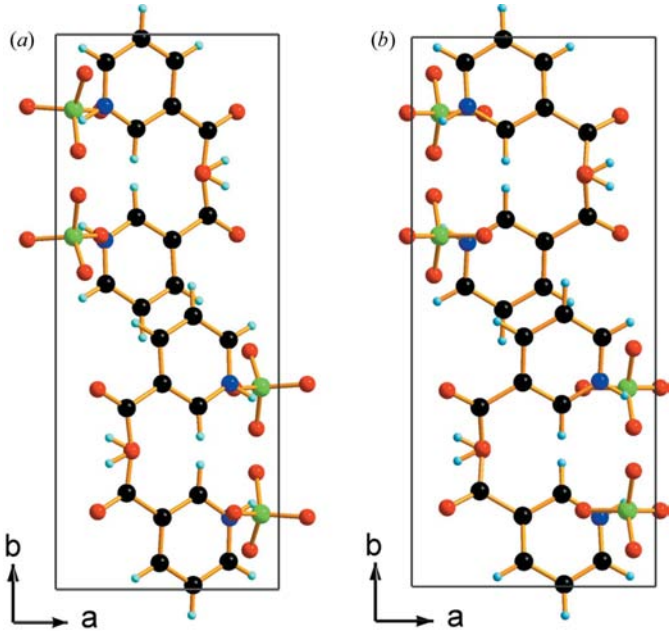

Figure 3
Cell-packing diagrams of (I) viewed down the c axis at (a) 148 K and (b) 103 K when β was chosen as 100.25° (reduced cell).

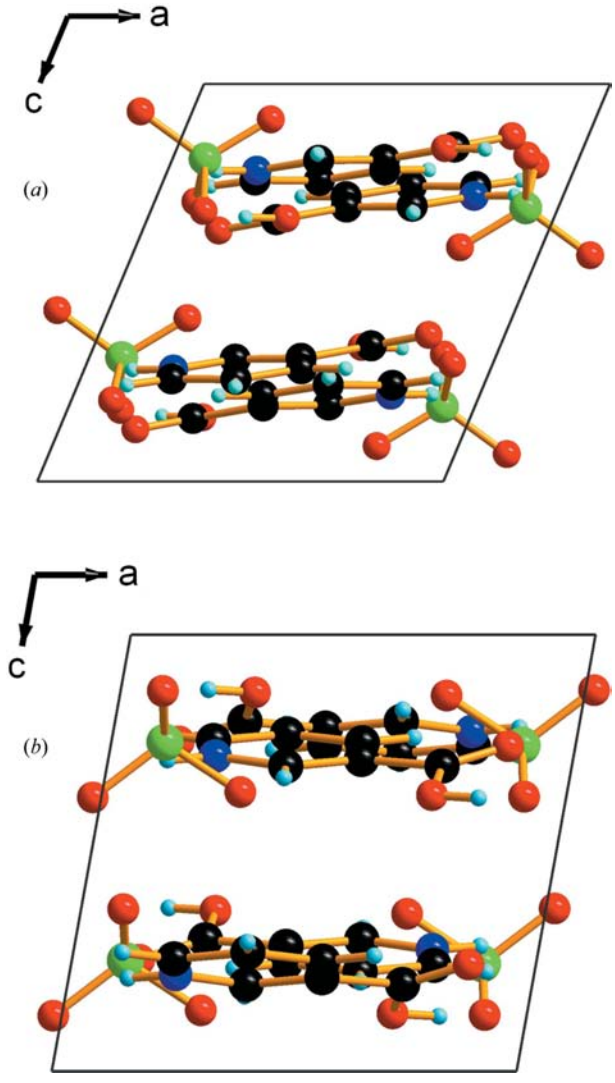

Figure 4
Cell-packing diagrams of (I) viewed down the b axis at (a) 148 K and (b) 103 K when β was chosen as 100.25° (reduced cell).

perchlorates are completely different and tilts of planar ions change sign. Therefore, the LT structure with the second unit-cell setting (a = 7.40, b = 16.79, c = 7.75 Å and β = 79.75°) matches better with the HT structure.

The order of this isosymmetric transition can be ascertained by measuring the unit-cell parameters against temperature. All the cell parameters show abrupt changes at 129 K, which are more pronounced for the β angle (Fig. 9*a*) and the c axis

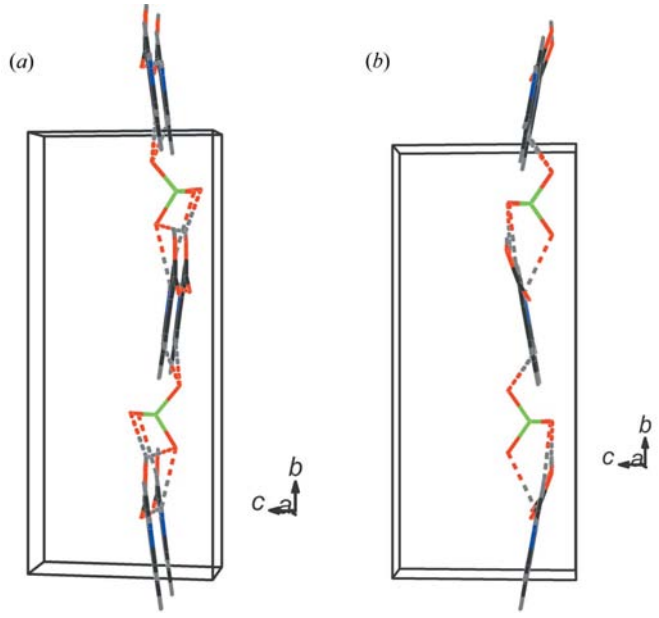

Figure 5
Diagrams of one hydrogen-bonded layer of (I) viewed parallel to the pyridinium ring planes (*a*) at 148 K and (*b*) 103 K when β was chosen as 100.25° (reduced cell).

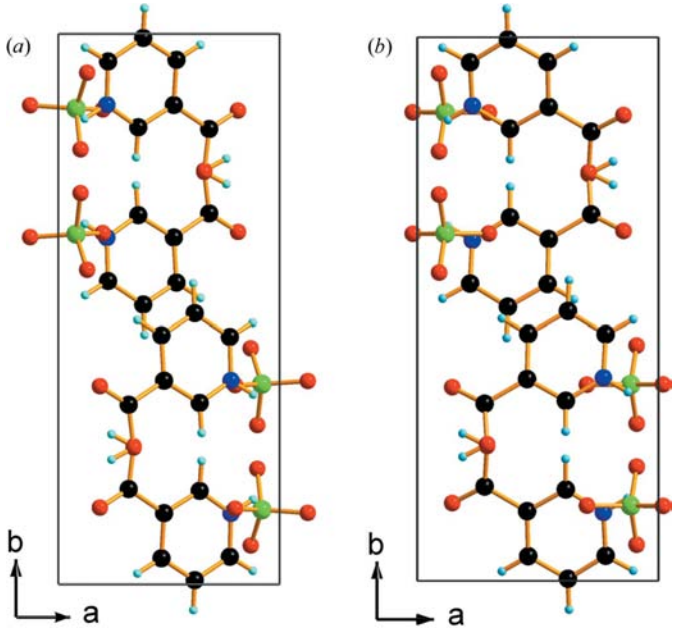

Figure 6
Diagrams of cell packing of (I) viewed down the c axis (*a*) at 148 K and (*b*) 103 K when β was chosen as 79.75°.

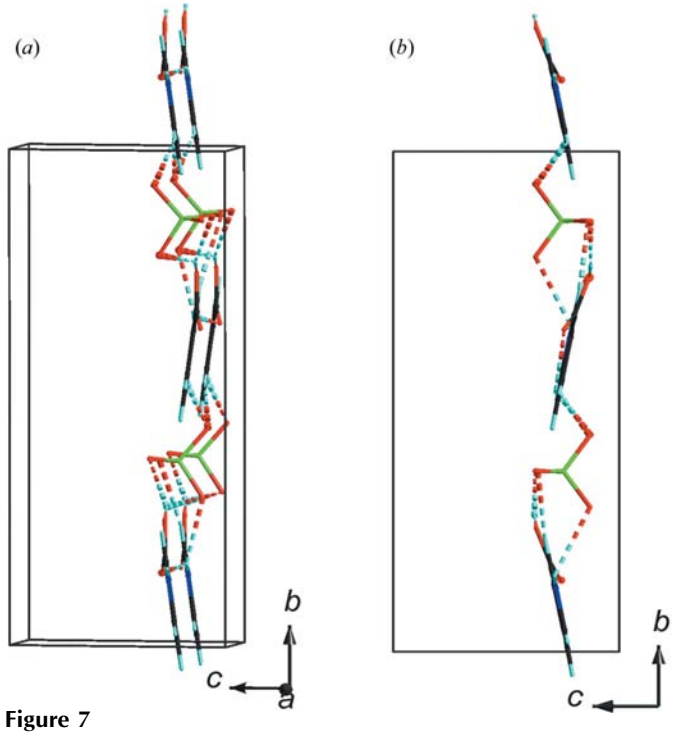

Figure 7
Packing diagrams at (*a*) 148 K and (*b*) 103 K of (I) viewed parallel to the pyridinium ring planes when β was chosen as 79.75°.

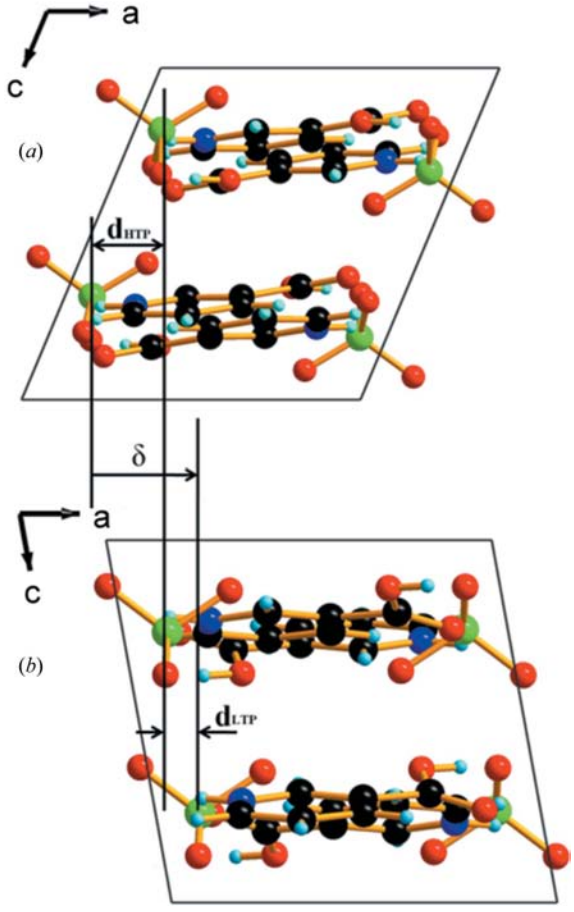

Figure 8
Packing diagrams of (I) at (*a*) 148 K and (*b*) 103 K viewed down the b axis.

(Fig. 9*b*), revealing a reversible first-order phase transition at T_c = 129 K.

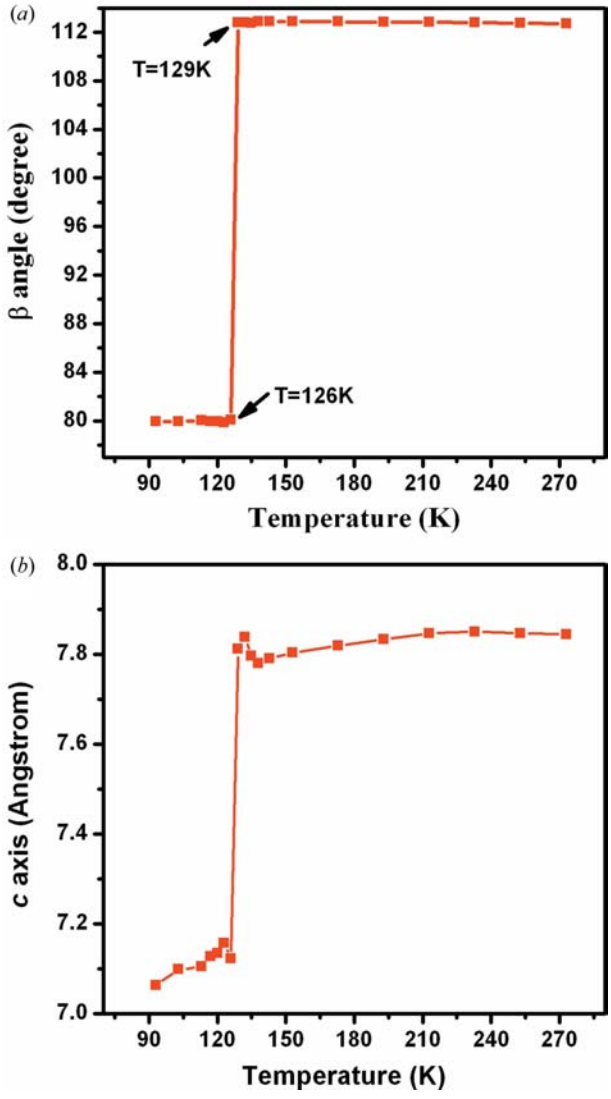

Figure 9
Temperature dependence of (*a*) the β angle and (*b*) the *c* axis in the range from 93 to 273 K.

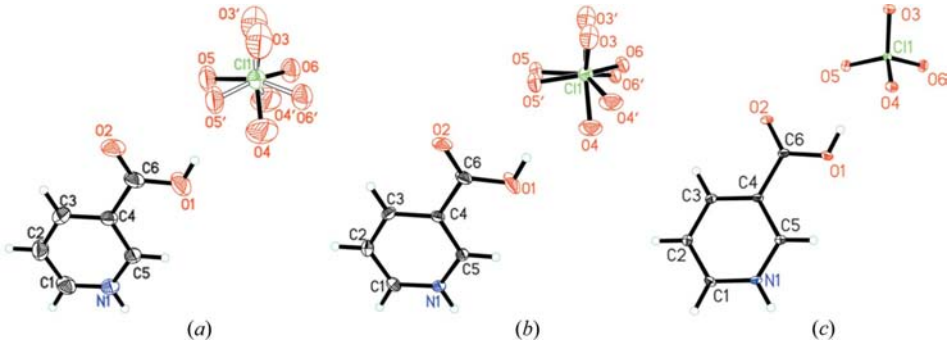

Figure 10
View of the asymmetric unit of (I) with atomic numbering scheme (*a*) at 298, (*b*) 148 and (*c*) 103 K. Displacement ellipsoids were drawn at the 30% probability level.

The components of the asymmetric units are the same in the HTP and the LTP. Each asymmetric unit contains a pyridinium-3-carboxylic acid cation and a perchlorate anion (Fig. 10). The bond distances and bond angles for the cation are in normal ranges (Jebas *et al.*, 2006; Athimoolam & Rajaram, 2005*a*,*b*; Athimoolam *et al.*, 2005; Slouf, 2001) and similar at the three temperatures. The dihedral angles between the planes of the carboxyl group and pyridinium ring are 12.03 (8), 9.37 (45) and 10.88 (56)° at 103, 148 and 298 K, showing no significant differences. The location of the cation in the HTP remains unchanged between 148 and 298 K with the corresponding atoms having similar positions. The perchlorate anion in the LTP at 103 K is ordered and has an almost ideal tetrahedral geometry. The anion in the HTP is disordered over two orientations with site-occupancy factors of 0.832 (4) and 0.178 (4) at 148 K, 0.809 (3) and 0.191 (3) at 298 K. The major parts at 148 and 298 K have the same orientation and the corresponding atoms have similar coordinates. The average distance of 0.70 (2) Å between the two parts of each O atom of the disordered perchlorate anion at 148 K is distinctly shorter than that of 1.26 (3) Å at 298 K, which shows that the perchlorate anion tends to become more ordered as the temperature decreases. As checked by *PLATON* (Spek, 2003), the orientation of the major parts of the perchorate anions is conducive to the formation of hydrogen bonds to the pyridinium-3-carboxylic acid cations. Fig. 11 shows a diagram of hydrogen-bonding interactions between the disordered anion and the cations at 298 K. In the main part of the perchlorate anion all the O atoms are linked to the H atoms by hydrogen bonds, while in the minor part one O atom is not linked to any H atom. Thus, the orientation of the major part should be more thermodynamically stable.

In the structure of (I) pyridinium-3-carboxylic acid cations related by the translation along the *a* axis are linked by N—H···$O_{carbonyl}$ hydrogen bonds to form one-dimensional chains. The perchlorate anions run between the chains which are related by a 2_1 screw axis and the anions link the chains by O—H···O, N—H···O and C—H···O hydrogen bonds (Table 2) to form well separated infinite layers parallel to the (001) plane (Fig. 12). For the structures of the hydrogen-bonded chains in the HTP and LTP, the notable difference is the distance between the pyridinium ring planes of the cations adjacent along the *a* axis. The distance in the HTP at 148 K is 0.6036 (1) Å. In the LTP at 103 K the adjacent pyridinium rings are almost coplanar with the distance reduced to 0.1271 (1) Å (Fig. 7). There is also a small decrease of the N···O distance and an increase of the N—H···O angle [N···O 2.825 (4), 2.7760 (19) Å; N—H···O 138.7, 145.1° at 148 and 103 K], which implies that the hydrogen bonds in the LTP are stronger.

To calculate the relative displacement between the hydrogen-

Table 2
Hydrogen-bond geometry (Å, °) at 103, 148 and 298 K.

D—H···A	D—H	H···A	D···A	D—H···A
103 K				
O1—H1···O4	0.84	1.96	2.7540 (17)	157
N1—H1A···O2^{i}	0.88	2.01	2.7760 (19)	145
N1—H1A···O5^{i}	0.88	2.53	3.0151 (19)	116
C1—H1B···O6^{ii}	0.95	2.39	3.227 (2)	147
C3—H3A···O6^{iii}	0.95	2.44	3.304 (2)	151
C5—H5A···O3^{i}	0.95	2.38	3.298 (2)	164
148 K				
O1—H1···O4	0.84	2.05	2.796 (4)	147
O1—H1···O5	0.84	2.35	3.092 (5)	148
N1—H1A···O2^{i}	0.88	2.10	2.825 (4)	139
N1—H1A···O5^{i}	0.88	2.35	2.976 (4)	128
C1—H1B···O6^{ii}	0.95	2.33	3.211 (5)	154
C3—H3A···O6^{iii}	0.95	2.33	3.263 (4)	168
C5—H5A···O3^{i}	0.95	2.52	3.427 (4)	160
298 K				
O1—H1···O4	0.82	2.15	2.874 (7)	147
O1—H1···O5	0.82	2.28	3.011 (6)	148
N1—H1A···O2^{i}	0.86	2.12	2.831 (4)	140
N1—H1A···O5^{i}	0.86	2.41	3.024 (5)	129
C1—H1B···O6^{ii}	0.93	2.38	3.240 (5)	154
C3—H3A···O6^{iii}	0.93	2.43	3.349 (5)	168
C5—H5A···O3^{i}	0.93	2.57	3.465 (6)	162
O1—H1···O5$'^{i}$	0.82	2.08	2.877(4)	163
C1—H1B···O6$'^{ii}$	0.93	2.51	3.206(4)	132
C5—H5A···O3$'^{i}$	0.93	2.46	3.344 (5)	158

Symmetry codes: (i) $x+1, y, z$; (ii) $-x+1, y-\frac{1}{2}, -z+\frac{1}{2}$; (iii) $-x, y-\frac{1}{2}, -z+\frac{1}{2}$.

bonded layers along the a axis that occurs during the phase transition, one can choose any pair of atoms related by glide-reflection symmetry like Cl1A and Cl1B (see Fig. 8). The Cl1A atom [0.07996 (9), 0.864201 (4) and 0.18835 (9)] is located on the right of Cl1B [0.07996 (9), 0.63580 (4) and 0.68835 (9)] and the distance between them along the a axis is *ca* 2.10 Å in the HTP, while in the LTP Cl1A [0.11554 (5), 0.86157 (2) and 0.25342 (5)] is located on the left of Cl1B [0.11554 (5), 0.63843 (2) and 0.75342 (5)] and the distance along the a axis is *ca* 0.63 Å. Therefore, a large relative displacement $\delta \simeq 2.73$ Å along the a axis occurs during the phase transition. The wide thermal hysteresis during the transition reflects such large structural changes.

3.4. Phase transition mechanism

A precise analysis of the main structural differences and the changes of the intermolecular interactions between the LTP and HTP is needed to find a primary order parameter or driving force and to identify the phase-transition mechanism. It is known that an order–disorder transition is one of the origins of the phase transitions. It would be typical of an order–disorder transition that the order parameter, representing the extent of order (ranging from zero for disorder to one for full order), would be zero above the transition and rise toward one below the transition, which is the case for KDP (Nelmes *et al.*, 1985). The perchlorate anion in (I) is typically disordered in two orientations at 298 K and even at 148 K (Fig. 10). Two parts can be located from the difference-Fourier map explicitly. They show a tendency to order with a decrease in temperature and change from 67% ordered to fully ordered through the transition. Therefore, the degree of order of the perchlorate anions seemingly does not have the characteristics of the order parameter of a typical order–disorder transition. Also, a disorder–order phase transition is often accompanied by symmetry breakage. In this case, the phase transition is isosymmetric. It is possible that the parameter describing the degree of order of the perchlorate anions is a secondary rather than primary order parameter, and that the order–disorder of the perchlorate anion is not the driving force.

Since the two most notable differences between the structures of the HTP and LTP are the change in distance between the adjacent pyridinium ring planes and the relative displacement between the hydrogen-bonded layers (Figs. 7 and 8), the forces leading to such changes will be the driving forces of the phase transition. For the hydrogen-bonded pyridinium-3-carboxylic acid cations in the HTP, the orientations remain almost unchanged upon lowering the temperature from 298 to 148 K. So does the distance [0.5337 (1) Å at 298 K, 0.6036 (1) Å at 148 K] between the adjacent pyridinium ring planes. Corresponding to this, the N—H···O hydrogen-bonding interactions show no distinct change with a decrease in temperature [N···O 2.831 (4), 2.825 (4) Å; 139.5, 138.7° at 298 and 148 K]. Actually, the reorientation of the cations occurs during the phase transition, resulting in a sudden decrease of the distance between the adjacent pyridinium ring planes [from 0.6036 (1) Å at 148 K to 0.1271 (1) Å at 103 K]. According to the main idea of the Landau theory of phase transitions, the order parameter is zero above T_c. The phase transition observed corresponds to a change in the order parameter from a zero value to a nonzero value occurring at T_c (Authier, 2003). Here we propose the primary order parameter η of the transition. η is defined as $\eta = (d_{HTP} - d)/$

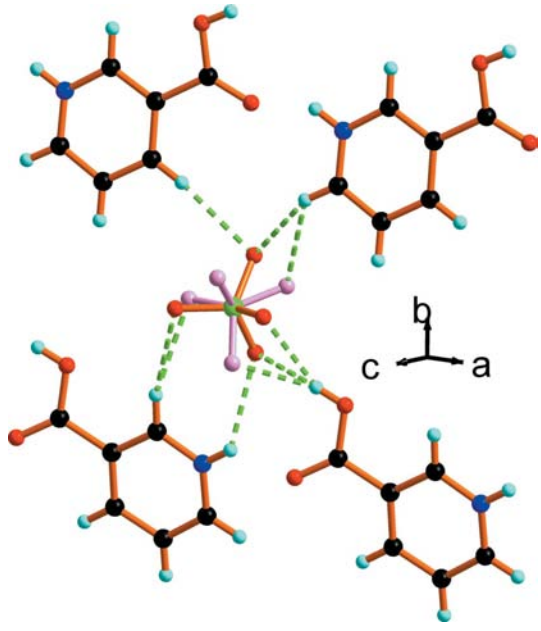

Figure 11
Diagram of hydrogen-bonding interactions between the disordered perchlorate anion and the pyridinium-3-carboxylic acid cations.

($d_{HTP} - d_{LTP}$), where d is the distance between the adjacent pyridinium ring planes, representing the degree of decrease in the distance between the adjacent pyridinium ring planes or the reorientation of the cations during the phase transition. With the decrease of the distance between the adjacent pyridinium ring planes, the hydrogen-bonding interactions within the chains become a little stronger. Therefore, the reorientation of the cations leads the system into a thermodynamically more stable state and the driving force of the phase transition is the reorientation of the cations.

As for the relative displacement between the hydrogen-bonded layers, it may be caused by steric effects arising from changes in the orientations of the pyridinium-3-carboxylic acid cations. Since the relative displacement δ is 2.63 Å, we can move one layer by 2.63 Å backward to obtain a structure in which the transition of the system is incomplete, at which point the coplanarity of the adjacent pyridinium rings is complete, but the relative displacement between the layers is not. In such an imaginary critical structure, unreasonable steric effects are obvious (Fig. 13). For example, the distances $O5^{iv}$—C5 [symmetry code: (iv) $1+x, \frac{1}{2}-y, \frac{1}{2}+z$], $O6^{iv}$—C5, $O6^{iv}$—N1 are 3.54, 3.85, 3.03 Å in the LTP. However, they would be 2.40, 2.84 and 2.89 Å in the imaginary critical structure, indicating short intermolecular contacts.

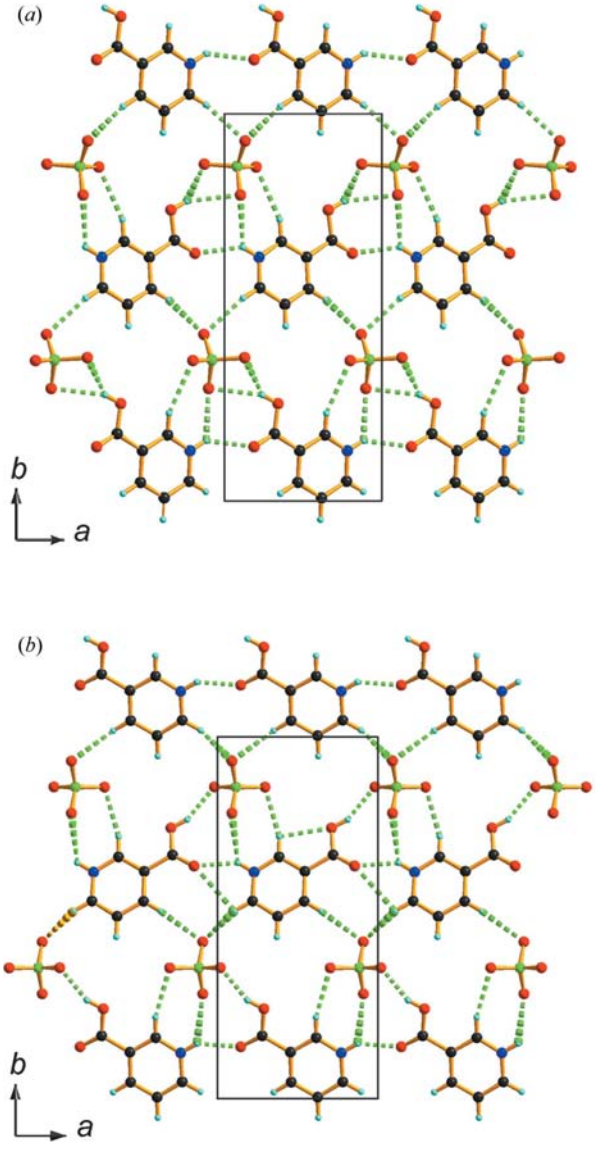

Figure 12
Packing diagrams at (*a*) 148 and (*b*) 103 K of (I) viewed down the *c* axis. The dashed lines show the hydrogen bonds presented in Table 2.

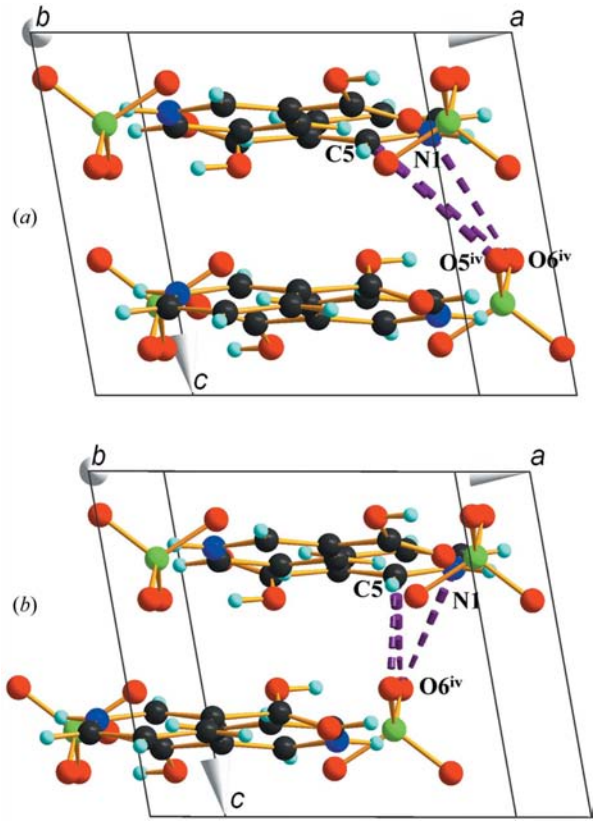

Figure 13
Packing diagrams of (*a*) the LT structure and (*b*) the imaginary critical structure by moving one layer of the LT structure backward of (I)

4. Conclusion

This paper reports an unusual structural phase transition of pyridinium-3-carboxylic acid perchlorate at ~129 K with large changes in the cell parameters. Although the phase transition mechanism involving a slight tilting of the cations but a large relative displacement between layers seems to be preferred, there is not enough information[2] to rule out another kind of mechanism, for example, the perchlorate ions reorient and the tilts of the pyridinium-3-carboxylic acid

[2] The relationship between the origins of the cells of the HTP and LTP is uncertain because a translation of *a*/2, *b*/2 and/or *c*/2 is possible and because any of the 2/*m* symmetry operations may be applied to the unit cell chosen. It is assumed that the correct relationship minimizes the atomic shifts associated with the transition, but in this pair of phases this condition does not lead to a unique relationship.

cations change sign. The driving forces are thought to be the reorientations of the pyridinium-3-carboxylic acid cations. Although the changes of the hydrogen-bonding interactions are the result of the transition, such a result is actually the thermodynamic condition for the transition. This example shows that the structural phase transitions of hydrogen-bonding molecular crystals still have many new features worthy of in-depth study.

The authors would like to thank the referee, co-editor and editor for their instructive comments and assistance on the technical writing. This work was supported by the National Natural Science Foundation of China (20973037, 20931002 and 90922005) and JiangSu Province NSF BK200802.

References

Athimoolam, S., Anitha, K. & Rajaram, R. K. (2005). *Acta Cryst.* E**61**, o2553–o2555.
Athimoolam, S. & Rajaram, R. K. (2005*a*). *Acta Cryst.* E**61**, o2674–o2676.
Athimoolam, S. & Rajaram, R. K. (2005*b*). *Acta Cryst.* E**61**, o2764–o2767.
Authier, A. (2003). Editor. *International Tables for Crystallography*, Vol. D. Dordrecht: Kluwer Academic Publishers.
Brandenburg, K. & Putz, H. (2005). *DIAMOND*, Version 3.0a. Crystal Impact GbR, Bonn, Germany.
Chantrapromma, S., Fun, H. K. & Usman, A. (2006). *J. Mol. Struct.* **789**, 30–36.
Chen, L.-Z., Zhao, H., Ge, J.-Z., Xiong, R.-G. & Hu, H.-W. (2009). *Cryst. Growth Des.* **9**, 3828–3831.
Horiuchi, S., Ishii, F., Kumai, R., Okimoto, Y., Tachibana, H., Nagaosa, N. & Tokura, Y. (2005). *Nat. Mater.* **4**, 163–166.
Horiuchi, S., Kumai, R. & Tokura, Y. (2007). *Chem. Commun.* pp. 2321–2329.
Jebas, S. R., Balasubramanian, T. & Light, M. E. (2006). *Acta Cryst.* E**62**, o3481–o3482.
Katrusiak, A. & Szafranski, M. (1999). *Phys. Rev. Lett.* **82**, 576–579.
Katrusiak, A. & Szafranski, M. (2006). *J. Am. Chem. Soc.* **128**, 15775–15785.
Kumai, R., Horiuchi, S., Sagayama, H., Arima, T.-H., Watanabe, M., Noda, Y. & Tokura, Y. (2007). *J. Am. Chem. Soc.* **129**, 12920–12921.
Nelmes, R. J., Kuhs, W. F., Howard, C. J., Tibballs, J. E. & Ryan, T. W. (1985). *J. Phys. Solid State Phys.* **18**, L711–L716.
Rigaku (2005). *CrystalClear*. Rigaku Corporation, Tokyo, Japan.
Sheldrick, G. M. (2008). *Acta Cryst.* A**64**, 112–122.
Slouf, M. (2001). *Acta Cryst.* E**57**, o61–o62.
Spek, A. L. (2003). *J. Appl. Cryst.* **36**, 7–13.
Steiner, Th. (1996). *Cryst. Rev.* **6**, 1–57.
Szafranski, M., Katrusiak, A. & McIntyre, G. J. (2002). *Phys. Rev. Lett.* **89**, 215507-1–215507-4.
Usman, A., Chantrapromma, S. & Fun, H.-K. (2001). *Acta Cryst.* C**57**, 1443–1446.